Dalton Transactions

RSC Publishing

PAPER

View Article Online
View Journal | View Issue

Cite this: *Dalton Trans.*, 2013, **42**, 1921

Two-step self-assembly of iron oxide into three-dimensional hollow magnetic porous microspheres and their toxic ion adsorption mechanism†

Yong Jia,[a,b] Xin-Yao Yu,[a] Tao Luo,[a] Mei-Yun Zhang,[a] Jin-Huai Liu[a] and Xing-Jiu Huang*[a]

Received 27th September 2012,
Accepted 1st November 2012

DOI: 10.1039/c2dt32522e

www.rsc.org/dalton

Hollow magnetic porous Fe_3O_4/α-FeOOH microspheres, with abundant surface hydroxyl groups and carbonate-like species, were prepared using a simple template free solution method. The obtained magnetic microspheres were characterized by field emission scanning electron microscopy, transmission electron microscopy, nitrogen adsorption–desorption isotherms, vibrating sample magnetometry and X-ray diffraction. A two-step self-assembly mechanism for the microspheres was proposed based on the morphology of the products produced with different reaction times and the X-ray diffraction of the raw product grown at the initial stage. The toxic ion adsorption properties of the microspheres were investigated for As(v), Cr(vi), Cd(ii) and Hg(ii) ion removal. The adsorption mechanism was studied by an X-ray photoelectron spectrometer and Fourier transform infrared absorption spectroscopy . The results suggest that both the surface hydroxyl groups and the carbonate-like species participated in the ion-exchange process.

Introduction

Recently, the removal of toxic ions from drinking water has attracted great attention because of their toxicity to the human health. Adsorption has been proven to be a promising technology for the purification of water with trace levels of toxic ions. Metal oxide adsorbents have been widely reported for toxic ion removal from water.[1] In particular, iron oxides have attracted great interest owing to their effective performance, low cost and natural abundance.[2–5] According to the adsorption mechanism, the surface hydroxyl groups of metal oxide adsorbents play a key role in the removal process. Therefore, oxyhydroxides, with abundant hydroxyl groups, have attracted great attention in toxic ion adsorption. Therefore, α-FeOOH presents a very important potential application for toxic ion removal owing to its low cost and environmental safety.[6–8]

Furthermore, the separation of the adsorbents from the purified water is also important for practical water treatment applications. Therefore, Fe_3O_4 and Fe_3O_4 based nanoadsorbents have also been widely utilized for water treatment owing to their magnetic properties.[5,9–13] In our previous work, γ-AlOOH@SiO_2/Fe_3O_4 porous magnetic microspheres, with a high Pb(ii) adsorption capacity, were synthesized by a template-induced method.[13] Recently, we reported a shaped-controlled synthesis of $CdCO_3$ microcrystals using a simple solution strategy and the corresponding nanoporous CdO was obtained.[14] Herein, using similar method, hollow magnetic porous Fe_3O_4/α-FeOOH microspheres, with abundant surface hydroxyl and carbonate-like groups, were prepared by a simple template free one-step solution method. The obtained magnetic microspheres present good adsorption properties for As(v), Cr(vi), Cd(ii), and Hg(ii). The adsorption mechanism was also studied in detail and the results suggest that the surface hydroxyl groups play an important role in removing toxic ions. In particular, the surface carbonate-like groups also participated in the ion-exchange process based on the results of the Fourier transform infrared spectroscopy and X-ray photoelectron spectroscopy.

[a]*Research Center for Biomimetic Functional Materials and Sensing Devices, Institute of Intelligent Machines, Chinese Academy of Sciences, Hefei 230031, P. R. China. E-mail: xingjiuhuang@iim.ac.cn; Fax: +86 551 5592420; Tel: +86 551 5591142*
[b]*Department of Pharmacy, Anhui University of Traditional Chinese Medicine, Hefei 230031, P. R. China*

†Electronic supplementary information (ESI) available: XRD patterns of the intermediate products synthesized at the initial stage, TEM images of the nanosheets, SEM images of the products prepared without EG. SEM images of the products synthesized with different volume ratios and concentrations. See DOI: 10.1039/c2dt32522e

Experimental section

Materials

All the chemicals used were analytical grade and were purchased from Shanghai Chemical Reagents Company and used without further purification. The As(v) and Cr(vi) stock solutions were prepared with deionized water using $Na_3AsO_4 \cdot 12H_2O$ and K_2CrO_4, respectively. $Hg(NO_3)_2$ and $Cd(NO_3)_2$ were used to prepare the Hg(ii) and Cd(ii) stock solutions, respectively. The pH value of the As(v) solution was not adjusted. The pH value of the Cr(vi) stock solutions were adjusted to 6.5 by the addition of HNO_3. The pH value of the Hg(ii) and Cd(ii) stock solutions were adjusted to 5. The toxic ion working solutions were freshly prepared by diluting the stock solutions with deionized water. The concentrations of the toxic ion species were given as elemental concentrations in this study.

Adsorbent preparation

In a typical synthesis protocol, a certain amount of $FeSO_4 \cdot 7H_2O$ was dissolved in a mixture of deionized water and ethylene glycol (EG) at room temperature. The concentration of the Fe^{2+} ions was 0.1 mol L^{-1}. After that, urea was added to the above solution and its concentration was 0.4 mol L^{-1}. After stirring for 10 minutes, the above solution was transferred into a conical flask with a stopper, heated at 100 °C for 12 h and then allowed to cool to room temperature naturally. The resulting brown precipitates were separated with a magnet, washed with distilled water and absolute alcohol several times and finally dried in an oven at 80 °C for 6 h.

Characterization

The as-prepared adsorbent was characterized by field emission scanning electron microscopy (SEM, FEI Sirion 200 FEG, operated at 10 kV), transmission electron microscopy (TEM, JEOL-2010, operated at 200 kV), X-ray diffraction (XRD, X'Pert ProMPD, Cu–Kα radiation, wavelength 1.5418 Å), Fourier transform infrared spectroscopy (FTIR, Nicolet Analytical Instruments, NEXUS-870) and X-ray photoelectron spectroscopy (XPS, VG ESCALAB MKII spectrometer, Mg KR X-ray source, 1253.6 eV, 120 W) analyses. The specific surface area and gas adsorption isotherms of the adsorbent was tested on a Coulter Omnisorp 100CX Brunauer–Emmett–Teller (BET) using nitrogen adsorption with a degassing temperature of 80 °C. The obtained Fe_3O_4/α-FeOOH adsorbents after toxic ion adsorption were also characterized by FTIR, XPS and TEM combined with energy dispersive X-ray (EDX).

Adsorption experiments

Batch adsorption experiments were conducted to examine the adsorption isotherm of the toxic ions. The adsorption experiments were carried out in 15 mL polypropylene flasks containing 10 mL of the arsenate solution and 0.01 g of the adsorbent. The flasks were then shaken at 150 r min^{-1} in a shaker at 25 °C for 24 h. In order to evaluate the adsorption properties of the adsorbent in a practical water treatment application, in the adsorption isotherm experiment, arsenate solutions with different concentrations were prepared without any pH value adjustment. After the adsorption experiments, the adsorbent was separated from the solution by a magnet and the residual toxic ion concentration in solution was determined using an inductively coupled plasma atomic emission spectrometer (Jarrell-Ash model ICAP 9000). To explore the competitive effects of various coexisting ions (Na^+, Mg^{2+}, Ca^{2+}, Al^{3+}, Cu^{2+}, and Pb^{2+}) on the removal of Cd(ii), 10 mL of 99.67 mg L^{-1} Cd(ii) solutions, each containing various components with 100 mg L^{-1} and 10 mg of the adsorbent, were shaken at pH 5. After the adsorption reached equilibrium, the adsorbent was separated *via* an external magnetic field and the supernatant was collected for metal concentration measurements.

Results and discussion

Structures of the Fe_3O_4/α-FeOOH adsorbent

Fig. 1a presents FESEM images of the as-prepared products. Nearly monodispersed three-dimensional (3D) microspheres about 6–7 μm in diameter were obtained. A broken microsphere, shown in Fig. 1b, suggests that the obtained microspheres are hollow and result from the self-assembly of nanosheets. The obtained microspheres were further characterized by TEM and the results are shown in Fig. 1c and d. The results further confirm that the hollow microspheres resulted from the self-assembly of nanosheets. The width of the nanosheets is about 200–300 nm. Furthermore, the nanosheets are composited of nanoneedles, as shown in Fig. 1d. The width of the nanoneedles is about 20–30 nm. In addition, many pores with a diameter below 4 nm were observed, as shown in the inset of Fig. 1d. Therefore, the nanosheets result from the self-assembly of porous nanoneedles.

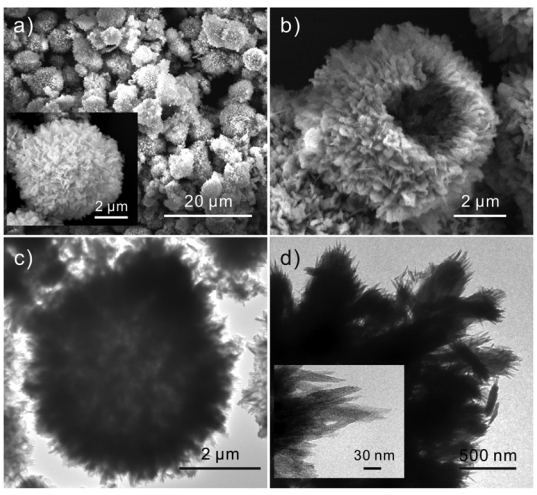

Fig. 1 FESEM (a, b) and TEM (c, d) images of the Fe_3O_4/α-FeOOH hollow microspheres.

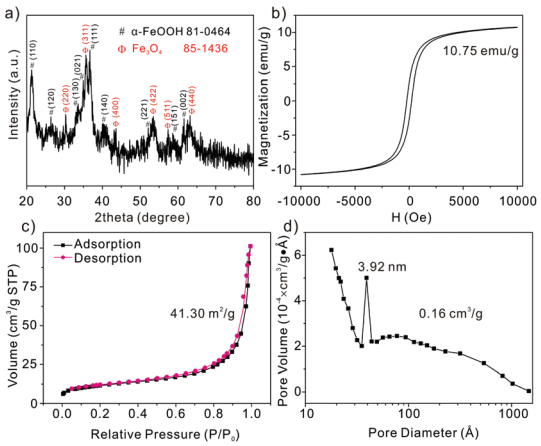

Fig. 2 XRD pattern (a), magnetic hysteresis loop (b), nitrogen adsorption–desorption isotherm (c), and the pore-size distribution curve (d) of the microspheres.

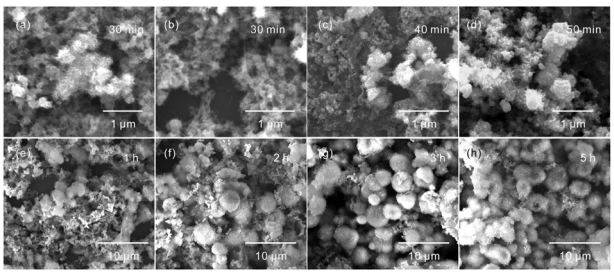

Fig. 3 SEM images of the intermediate products prepared at reaction times of 30 min (a, b), 40 min (c), 50 min (d), 1 hour (e), 2 hours (f), 3 hours (g), and 5 hours (h).

Fig. 2a presents the XRD pattern of the obtained microspheres. All of the diffraction peaks can be indexed to α-FeOOH (JCPDS 81-0464) and Fe_3O_4 (JCPDS 85-1436). Considering the presence of Fe_3O_4, the magnetic properties were also measured at room temperature and the magnetisation-hysteresis loop is shown in Fig. 2b. The hysteresis loop of the product shows ferromagnetic behavior with saturation magnetisation (M_s) of 10.75 emu g^{-1}. Though the M_s of the obtained microspheres is lower than the bulk Fe_3O_4, it is still promising for toxic ion removal. Fig. 2c and 2d show the nitrogen adsorption–desorption isotherm and the pore-size distribution curve, respectively. The BET surface area and BJH pore volume were 41.30 m^2 g^{-1} and 0.16 cm^3 g^{-1}, respectively. From Fig. 2d, a wide range distribution of the mesopores was observed and the mesopores, around 3.92 nm, may be derived from the pores shown in Fig. 1d.

To clarify the growth mechanism of the obtained Fe_3O_4/α-FeOOH microspheres, the structures of the intermediate products were studied and the results are shown in Fig. 3. After the initial 30 minutes, only a few yellow nonmagnetic products were formed. From Fig. 3a and b, the products were composited of nanoneedles, nanowires and their sphere-like aggregations. The XRD pattern (Fig. S1, ESI†) suggests that the above yellow colloidal product was $Fe_2O_3{\cdot}H_2O$ (JCPDS 02-0127). It is well known that, at high temperature, urea can be hydrolyzed in water and give off OH^-, CO_2 and ammonia, as shown in eqn (1). At the same time, part of the Fe^{2+} ion was oxidized to Fe^{3+} by dissolved oxygen in the water, as shown in eqn (2). Considering the solubility products of $Fe(OH)_3$ (pKsp 37.4) and $Fe(OH)_2$ (pKsp 15.1), the yellow $Fe_2O_3{\cdot}H_2O$ should be a result of the hydrolysis of the Fe^{3+} under high concentrations of OH^-, as shown in eqn (3). After prolonging the reaction time to 40 min, brown magnetic products were obtained. From Fig. 3c and 3d, nanospheres about 500 nm in diameter were observed. These nanospheres were clearly a result of the aggregation of small nanoparticles and nanosheets. The magnetic characteristics and the XRD pattern (Fig. S1, ESI†) of the products confirm the formation of Fe_3O_4. In this stage, the concentration of OH^- was increased with the hydrolyzation of urea. Therefore, the residual Fe^{2+} and the newly formed Fe^{3+} were hydrolyzed simultaneously and resulted in the formation of $Fe(OH)_2/Fe(OH)_3$. Then, the obtained $Fe(OH)_2/Fe(OH)_3$ was transformed into Fe_3O_4 nanoparticles, as shown in eqn (4).

After a reaction time of 1 hour, the diffraction peaks of Fe_3O_4 became strong, and on the contrary, the diffraction peaks of $Fe_2O_3{\cdot}H_2O$ became weak. On further prolonging the reaction time to 5 hours, the diffraction peaks of $Fe_2O_3{\cdot}H_2O$ disappeared and diffraction peaks for α-FeOOH were detected. In addition, from Fig. 3e to 3g, the diameter of the sphere-like products became larger. At the same time, the $Fe_2O_3{\cdot}H_2O$ nanoneedles and nanowires could not be observed, which means that the formed $Fe_2O_3{\cdot}H_2O$ was dissolved. In this process, owing to the hydrolysis of iron ions, the concentration of OH^- was decreased. The hydrolysis of Fe^{2+} became weak owing to the high solubility products of $Fe(OH)_2$. The hydrolysis of Fe^{3+} was the dominant reaction. Therefore, the amount of $Fe(OH)_3$ was larger than that of $Fe(OH)_2$. As a result, in the Fe_3O_4 formation process, the residual $Fe(OH)_3$ was transformed into α-FeOOH, as shown in eqn (5).[6,15] Then, the obtained $Fe(OH)_2/Fe(OH)_3$/α-FeOOH was transformed into Fe_3O_4/α-FeOOH, as shown in eqn (6). Finally, the Fe_3O_4/α-FeOOH microspheres were obtained.

$$(NH_2)_2CO + 3H_2O \rightarrow 2NH_4^+ + 2OH^- + CO_2 \quad (1)$$

$$4Fe^{2+} + O_2 + 2H_2O \rightarrow 4Fe^{3+} + 4OH^- \quad (2)$$

$$Fe^{3+} + OH^- \rightarrow Fe(OH)_3 \rightarrow Fe_2O_3 \cdot H_2O \quad (3)$$

$$Fe^{2+} + Fe^{3+} + OH^- \rightarrow Fe(OH)_2/Fe(OH)_3 \rightarrow Fe_3O_4 \quad (4)$$

$$Fe^{2+} + Fe^{3+} + OH^- \rightarrow Fe(OH)_2/Fe(OH)_3/\alpha\text{-FeOOH} \quad (5)$$

$$Fe(OH)_2/Fe(OH)_3/\alpha\text{-FeOOH} \rightarrow Fe_3O_4/\alpha\text{-FeOOH} \quad (6)$$

After 12 hours, the dispersed nanoparticles can barely be observed and microspheres, resulting from the self-assembly of nanosheets, were obtained. TEM images of the nanosheet (Fig. S2, ESI†) suggest that the nanosheets were a result of the self-assembly of the nanoparticles and nanoneedles. Therefore, the results suggest that the obtained hollow 3D

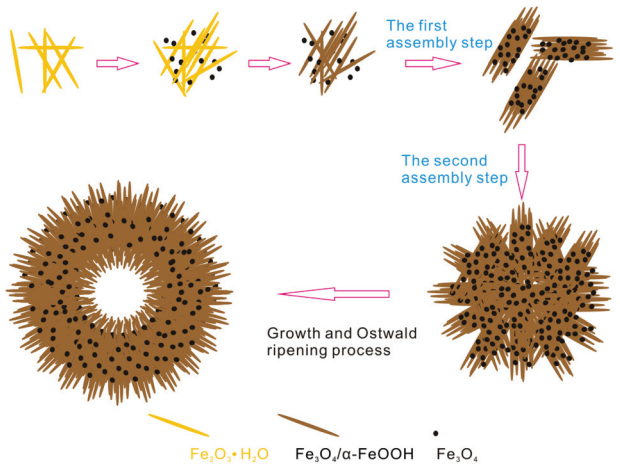

Fig. 4 Schematic description of the process for the growth of the hollow magnetic porous microspheres.

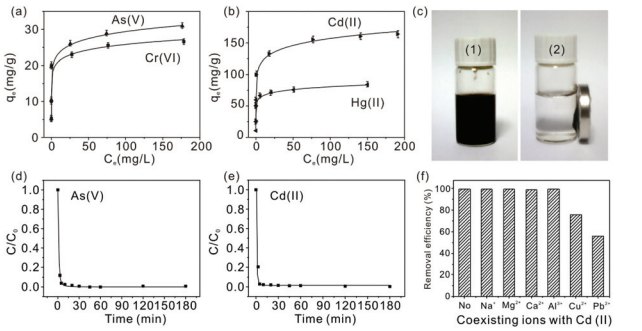

Fig. 5 (a, b) Adsorption isotherms of As(v), Cr(vi), Cd (ii) and Hg(ii). (c) The digital photographs of the aqueous solution of As(v) with dispersed Fe_3O_4/α-FeOOH microspheres (1) and the solution after magnetic separation using an external magnetic field (2). (d, e) Time-dependent concentration of As(v) (initial concentration of 20.25 mg L^{-1}) and Cd(ii) (initial concentration of 99.67 mg L^{-1}) using a Fe_3O_4/α-FeOOH adsorbent. (f) Effect of common ions (100 mg L^{-1}) on the removal of Cd(ii) by a Fe_3O_4/α-FeOOH adsorbent.

microspheres resulted from the two-step self-assembly of the Fe_3O_4 nanoparticles and the Fe_3O_4/α-FeOOH nanoneedles. More importantly, in the second self-assembly process, the core in the center of the microsphere was completely consumed, mainly through the Ostwald ripening process.[16–18] Based on the above discussion, a growth model of the hollow magnetic porous microsphere is schematically presented in Fig. 4.

The hollow magnetic porous microspheres were synthesized in a mixture of water and EG. EG has been used to mediate the morphology of nanomaterials.[5,19] SEM images of the product prepared without EG suggests that only cube-like products were obtained (Fig. S3, ESI†). To further study the roles of EG, the influence of the volume ratio of EG and water were investigated and the results are shown in Fig. S4.† Only a few of microspheres and large amount of nanowires were obtained with a volume ratio of 9 : 1 (Fig. S4a, ESI†). With a slightly increased volume of water, large microspheres of about 10 μm in diameter were synthesized (Fig. S4b, ESI†). Furthermore, a small amount of microspheres and some dispersed nanoneedle bundles were obtained with a volume ratio of 2 : 8 (Fig. S4c, d, ESI†). When the volume of water was further increased, some cube-like products coated with nanoneedles were obtained (Fig. S4e, f, ESI†). On comparison with the products prepared in pure water (Fig. S3, ESI†), it is clear that the growth of the nanoneedles can be attributed to the presence of EG. The results suggest that an appropriate amount of EG plays a key role in the formation of nanoneedles and the subsequent self-assembly to the hollow microspheres.

In addition, the concentration of the solution was also investigated. When the concentration of the ferrous sulfate solution was 0.05 mol L^{-1}, some small spheres were obtained (Fig. S5a, b, ESI†). With an increase of the concentration, the spheres became more and more uniform (Fig. S5c, d, ESI†). When the concentration of the ferrous sulfate was increased to 0.1 mol L^{-1}, nearly monodispersed microspheres were obtained. On further increasing the concentration to 0.2 mol L^{-1}, microspheres of less than 2 μm were prepared (Fig. S5e, f, ESI†). Therefore, the optimum concentration of the ferrous sulfate solution was 0.1 mol L^{-1}.

Toxic ion adsorption properties

Metal oxide adsorbents have been widely reported for toxic ion removal from water. Here, the adsorption properties of hollow magnetic porous Fe_3O_4/α-FeOOH microspheres for As(v), Cr(vi), Cd(ii) and Hg(ii) were investigated. As(v) adsorption experiments were performed without any pH adjustment as we believe that the adsorption capacities are more attractive in practical water treatment applications. The adsorption isotherms are shown in Fig. 5. With an equilibrium concentration less than 200 mg L^{-1}, the Langmuir maximum adsorption capacities of As(v) and Cr(vi) were 30.2 and 26.5 mg g^{-1}, respectively. From Fig. 5b, the maximum adsorption capacities of Cd(ii) and Hg(ii) were 164.5 and 79.5 mg g^{-1}. With the same equilibrium concentration, the adsorption capacity for As(v) is lower than that reported for pure α-FeOOH.[6] However, the adsorption capacities for As(v) and Cr(vi) are much higher than those of pure Fe_3O_4 hierarchical structures.[5] A comparison of the toxic ion adsorption properties of various iron oxides is summarized in Table 1.[5,6,10,20–22] Accordingly, these results definitely show that the as-prepared Fe_3O_4/α-FeOOH achieved good adsorption properties. Furthermore, the magnetic properties imply a magnetic responsivity of the microspheres, which enables them to be separated from solution by the application of an external magnetic force. A magnetic separation test for the Fe_3O_4/α-FeOOH microspheres can be seen in Fig. 5c.

Fig. 5d and e present the time-dependent concentration of As(v) and Cd(ii) with initial concentrations of 20.25 mg L^{-1} and 99.67 mg L^{-1}, respectively. It is clear that over 99.0% of the toxic ions have been removed at room temperature after about 15 min. Furthermore, the influence of the common cationic species on Cd(ii) removal was also studied and the results are shown in Fig. 5e. The results suggest that the presence of Na^+,

Table 1 Comparison of the toxic ion adsorption properties of various iron oxides

Adsorbents	S (m^2 g^{-1})	As(v) q_e	Cr(vi) q_e	Cd(ii) q_e	pH	Ref.
Fe_3O_4	34	4.65	4.38	—	4	5
α-Fe_2O_3	40	5.31	4.47	—	4	5
Fe_3O_4	102	44.1	—	—	3	10
Fe_3O_4	203.2	50	—	—	3	20
Fe_3O_4	203.2	20	—	—	7	20
α-FeOOH	103	4.7	—	—	5	21
α-FeOOH	121	66.2	—	—	Unadjusted	6
β-FeOOH	176	—	—	70.4	5	22
Fe_3O_4/α-FeOOH	41.3	30.2	26.5	164.5 (pH = 5)	Unadjusted	This work

Mg^{2+}, Ca^{2+} and Al^{3+} on the ion-exchange of Cd(ii) has almost no influence on Cd(ii) removal since they did not compete for the active surface. However, the removal efficiency was decreased to 75.66% owing to the presence of Cu^{2+}. Furthermore, the influence of Pb^{2+} was greater than that of Cu^{2+}. These results mean that competition from other heavy-metal ions cannot be ignored, which should result from a similar ion-exchange process.

Adsorption mechanism

To reveal the adsorption mechanism, the Fe_3O_4/α-FeOOH adsorbent, before and after toxic ion adsorption, was characterized by FTIR and the results are shown in Fig. 6. For the Fe_3O_4/α-FeOOH adsorbent, the peak at 3401 cm^{-1} can be assigned to physically absorbed water. The peaks at 878 and 789 cm^{-1} are assigned to the Fe–O–H bending vibrations of α-FeOOH (δOH and γOH, respectively).[23] The peak at around 622 cm^{-1} is assigned to the Fe–O and Fe–OH stretching or lattice vibrations.[24,25] The stretching mode of the structural hydroxyl groups (νOH) of the product is located at 3263 cm^{-1}.[23] For the above FTIR peaks, no obvious changes were observed after As(v) and Cr(vi) adsorption. Based on the ion-exchange mechanism, As(v) and Cr(vi) adsorption were determined by the surface hydroxyl groups of the adsorbents. In Fig. 6a, the peaks at 1125, 1047 and 976 cm^{-1} are assigned to the surface hydroxyl groups.[26–28] After As(v) and Cr(vi) adsorption, these peaks clearly weakened. The results confirm the exchange between the surface hydroxyl groups and arsenate ions in solution, as well as Cr(vi). In addition, from Fig. 6a, the peaks at 1518, 1400 and 816 cm^{-1} were also weakened at the same time. In the present work, at high temperature, urea was decomposed and the formed CO_2 was dissolved in water. Therefore, the carbonate ions generated from the dissolved CO_2 resulted in nucleation upon mixing with the solution of iron.[15,29] In this process, the carbonate ions took part in the formation of the final products and formed $FeO(CO_3)^-$ on the adsorbent surface.[30] Therefore, the FTIR peaks at 1518, 1400 and 816 cm^{-1} are due to the carbonate-like species.[31–36] After As(v) and Cr(vi) adsorption, the above three peaks obviously weakened. These results mean that the carbonate-like groups also participated in the ion-exchange process.

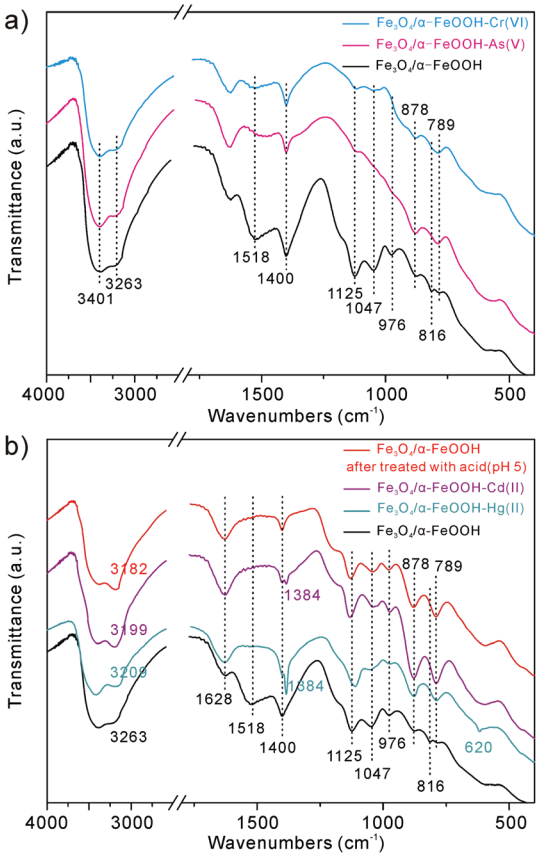

Fig. 6 FTIR spectra of the Fe_3O_4/α-FeOOH adsorbent before and after heavy-metal ion adsorption.

Fig. 6b shows the FTIR spectra of the adsorbent before and after Cd(ii) and Hg(ii) adsorption. The peak at 1384 cm^{-1} is ascribed to the vibration of NO_3^-, which was adsorbed on the surface.[28] For the surface hydroxyl group peaks, only the peak at 1047 cm^{-1} was slightly weakened after adsorption. At pH 5, protonation in the acid solution resulted in the formation of $FeOOH_2^+$ on the surface of the adsorbents. Therefore, the weakened FTIR peak at 1047 cm^{-1} suggests the existence of an ion exchange process between the protonated surface hydroxyl groups and the hydrolytic cations.[37–42]

At the same time, the FTIR peaks corresponding to the stretching vibration of the structural hydroxyl groups showed a

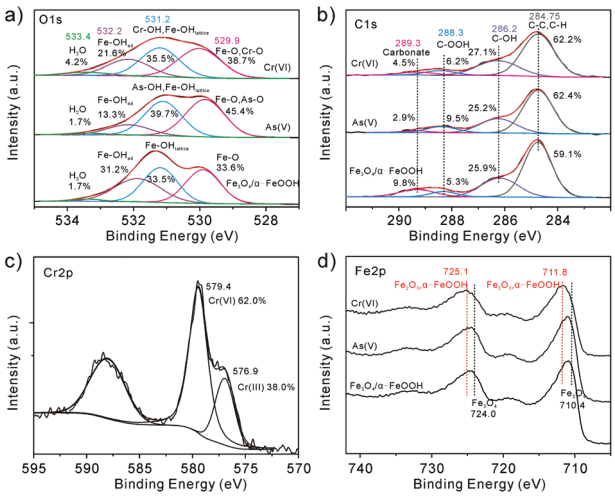

Fig. 7 XPS O1s (a), C1s (b), and Fe2p (d) spectra of the Fe_3O_4/α-FeOOH adsorbent before and after adsorption of As(v) and Cr(vi). XPS Cr2p (c) spectrum of the adsorbent after Cr(vi) adsorption.

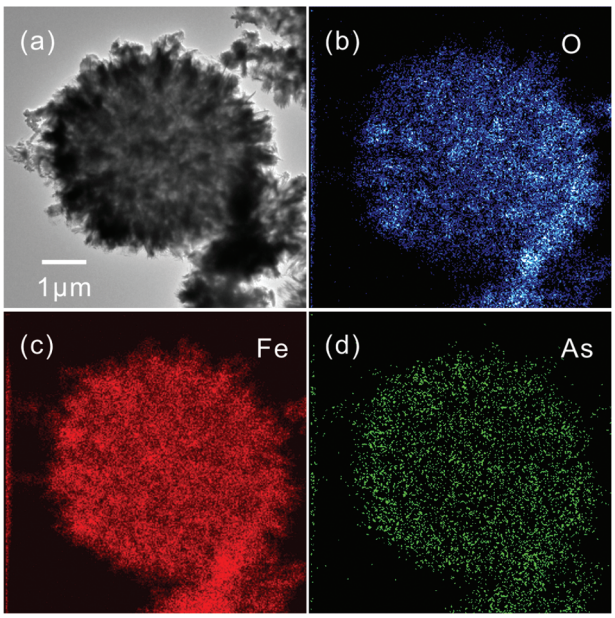

Fig. 8 TEM image (a) and elemental mapping images (b–d) of the microspheres after As(v) adsorption.

tendency to shift toward lower wave numbers, as shown in Fig. 6b. In addition, the peaks at 878 and 789 cm^{-1} clearly became stronger. These results may be attributed to the increased crystallinity.[23] A newly formed peak at 620 cm^{-1} after Hg(ii) adsorption may be a result of the Hg–O stretching vibration.[43] Furthermore, the peak at 1400 cm^{-1} obviously weakened and the peaks at 1518 and 816 cm^{-1} almost disappeared. To further investigate the role of the surface carbonate-like species on the cationic adsorption, the adsorbent was dispersed in a nitric acid solution of pH 5. After being shaken at 25 °C for 24 h, the adsorbent was characterized using FTIR and the results are shown in Fig. 6b. It is clear that the peak from the structural hydroxyl groups became stronger and shifted toward lower wavenumbers. The peaks at 878 and 789 cm^{-1} simultaneously became stronger. These results mean that the increased crystallinity of the adsorbent was due to the low pH value. In addition, the peaks at 1518 and 816 cm^{-1} disappeared and the peak at 1400 cm^{-1} obviously weakened. The results imply the existence of a reaction between the surface carbonate-like species and H^+ in solution. Therefore, the surface carbonate-like species may not participate in the cationic adsorption process.

In order to further investigate the proposed anion adsorption mechanism, the adsorbent was further characterized by XPS and the results are shown in Fig. 7. For the Fe_3O_4/α-FeOOH adsorbent, the O1s spectra, shown in Fig. 7a, suggests that four peaks are located at 529.9, 531.2, 532.2 and 533.4 eV, respectively. For the iron oxides, the peaks at 529.9 eV can be assigned to the lattice oxygen atoms binding with Fe (Fe–O).[44–47] The peak at 531.2 eV can be assigned to the lattice hydroxyl groups ($Fe–OH_{lattice}$) of α-FeOOH. The peaks at 532.2 and 533.4 eV can be assigned as adsorbed hydroxyl groups ($Fe–OH_{ad}$) and water (H_2O), respectively.[44,47,48] It is well known that, on the surface of Fe, the oxide film formed at ambient temperature has been suggested to contain primarily FeOOH.[48–50] In the formation process of the FeOOH, $Fe–OH_{ad}$ groups were generated on the surface after oxidation.[48] As a result, surface hydroxyl groups of FeOOH were formed. Therefore, the $Fe–OH_{ad}$ groups and the surface hydroxyl groups, determined by XPS and FTIR, respectively, were the same hydroxyl species.

From Fig. 7a, it is clear that the amount of the surface hydroxyl groups decreased after As(v) and Cr(vi) adsorption. In addition, from the C1s spectra shown in Fig. 7b, the peak at 289.3 eV can be assigned to the carbonate-like groups.[51] After As(v) and Cr(vi) adsorption, the contents of the carbonate-like groups obviously decreased. The results confirm the important role of the surface carbonate-like groups. Fig. 7c is the Cr2p spectrum of the adsorbent after adsorption of Cr(vi). The peak at 576.9 eV suggests the presence of Cr(iii),[52] which is a result of the reduction of Cr(vi) by Fe(ii) in Fe_3O_4/α-FeOOH. Fig. 7d presents the Fe2p spectra before and after the adsorption of As(v) and Cr(vi). No obvious changes were observed after As(v) adsorption. After Cr(vi) adsorption, the content of Fe(iii) was increased,[47,53,54] which is consistent with the existence of Cr(iii) after adsorption. The results also mean that the reduced Cr(vi) species was also adsorbed by the adsorbent. After As(v) adsorption, the adsorbent was investigated by TEM with EDX elemental analysis and the results are shown in Fig. 8. It is clear that the morphology of the microspheres was not changed. Elemental mapping images after As(v) adsorption suggest that the As atoms were uniformly dispersed in the microspheres.

Conclusions

Hollow magnetic porous Fe_3O_4/α-FeOOH microspheres, with abundant surface hydroxyl groups and carbonate-like species,

were prepared using a simple template free solution method. The growth process and the growth mechanism were investigated in detail. A novel two-step self-assembly mechanism was proposed for the growth of the microspheres. Toxic ion adsorption properties and the adsorption mechanism were studied. The surface hydroxyl groups play a key role in the cations adsorption. For the anions, the surface hydroxyl groups and the carbonate-like species simultaneously participated in the ion-exchange process. This study demonstrates the important role of the surface carbonate-like species and suggests the possibility of designing metal oxide nanoadsorbents with active surface carbonate-like species for anion adsorption.

Acknowledgements

This work was supported by a grant from the Natural Science Foundation of the Education Committee of Anhui Province (KJ2012A179), National Key Scientific Program, Nanoscience and Nanotechnology (Grant No. 2011CB933700), China Postdoctoral Science Foundation (2011M501073 and 20110490386), Anhui University of Traditional Chinese Medicine (2011zr017B) and the National Natural Science Foundation of China (21103198 and 21073197).

Notes and references

1 D. Mohan and C. U. Pittman, *J. Hazard. Mater.*, 2007, **142**, 1–53.
2 L. C. Roberts, S. J. Hug, T. Ruettimann, M. Billah, A. W. Khan and M. T. Rahman, *Environ. Sci. Technol.*, 2004, **38**, 307–315.
3 K. P. Raven, A. Jain and R. H. Loeppert, *Environ. Sci. Technol.*, 1998, **32**, 344–349.
4 J. Majzlan, *Environ. Sci. Technol.*, 2011, **45**, 4726–4732.
5 L. S. Zhong, J. S. Hu, H. P. Liang, A. M. Cao, W. G. Song and L. J. Wan, *Adv. Mater.*, 2006, **18**, 2426–2431.
6 H. Li, W. Li, Y. J. Zhang, T. S. Wang, B. Wang, W. Xu, L. Jiang, W. G. Song, C. Y. Shu and C. R. Wang, *J. Mater. Chem.*, 2011, **21**, 7878–7881.
7 B. A. Manning, S. E. Fendorf and S. Goldberg, *Environ. Sci. Technol.*, 1998, **32**, 2383–2388.
8 K. Amstaetter, T. Borch, P. Larese-Casanova and A. Kappler, *Environ. Sci. Technol.*, 2010, **44**, 102–108.
9 C. T. Yavuz, J. T. Mayo, W. W. Yu, A. Prakash, J. C. Falkner, S. Yean, L. L. Cong, H. J. Shipley, A. Kan, M. Tomson, D. Natelson and V. L. Colvin, *Science*, 2006, **314**, 964–967.
10 S. X. Zhang, H. Y. Niu, Y. Q. Cai, X. L. Zhao and Y. L. Shi, *Chem. Eng. J.*, 2010, **158**, 599–607.
11 G. Gao, H. X. Wu, W. J. Gao, Y. X. Zhang, P. Huang and D. X. Cui, *CrystEngComm*, 2011, **13**, 6950–6954.
12 V. Chandra, J. Park, Y. Chun, J. W. Lee, I. C. Hwang and K. S. Kim, *ACS Nano*, 2010, **4**, 3979–3986.
13 Y. X. Zhang, X. Y. Yu, Z. Jin, Y. Jia, W. H. Xu, T. Luo, B. J. Zhu, J. H. Liu and X. J. Huang, *J. Mater. Chem.*, 2011, **21**, 16550–16557.
14 Y. Jia, X. Y. Yu, T. Luo, J. H. Liu and X. J. Huang, *RSC Adv.*, 2012, **2**, 10251–10254.
15 N. K. Chaudhari, H. C. Kim, D. Son and J. S. Yu, *CrystEngComm*, 2009, **11**, 2264–2267.
16 Y. Wang, Q. S. Zhu and L. Tao, *CrystEngComm*, 2011, **13**, 4652–4657.
17 H. G. Yang and H. C. Zeng, *J. Phys. Chem. B*, 2004, **108**, 3492–3495.
18 X. Wang, F. L. Yuan, P. Hu, L. J. Yu and L. Y. Bai, *J. Phys. Chem. C*, 2008, **112**, 8773–8778.
19 X. C. Jiang, Y. L. Wang, T. Herricks and Y. N. Xia, *J. Mater. Chem.*, 2004, **14**, 695–703.
20 T. Tuutijarvi, J. Lu, M. Sillanpaa and G. Chen, *J. Hazard. Mater.*, 2009, **166**, 1415–1420.
21 P. Lakshmipathiraj, B. R. Narasimhan, S. Prabhakar and G. B. Raju, *J. Hazard. Mater.*, 2006, **136**, 281–287.
22 M. Mohapatra, L. Mohapatra, S. Anand and B. K. Mishra, *J. Chem. Eng. Data*, 2010, **55**, 1486–1491.
23 S. Krehula and S. Music, *J. Cryst. Growth*, 2008, **310**, 513–520.
24 P. Cambier, *Clay Miner.*, 1986, **21**, 191–200.
25 P. Cambier, *Clay Miner.*, 1986, **21**, 201–210.
26 Y. Zhang, M. Yang, X. M. Dou, H. He and D. S. Wang, *Environ. Sci. Technol.*, 2005, **39**, 7246–7253.
27 G. S. Zhang, H. J. Liu, R. P. Liu and J. H. Qu, *J. Hazard. Mater.*, 2009, **168**, 820–825.
28 G. S. Zhang, J. H. Qu, H. J. Liu, R. P. Liu and G. T. Li, *Environ. Sci. Technol.*, 2007, **41**, 4613–4619.
29 T. Sugimoto, *Adv. Colloid Interface Sci.*, 1987, **28**, 65–108.
30 B. Dutcher, M. Fan, B. Leonard, M. D. Dyar, J. Tang, E. A. Speicher, P. Liu and Y. Zhang, *J. Phys. Chem. C*, 2011, **115**, 15532–15544.
31 C. Li, Y. Sakata, T. Arai, K. Domen, K. Maruya and T. Onishi, *J. Chem. Soc., Faraday Trans. 1*, 1989, **85**, 929–943.
32 J. B. Harrison and V. E. Berkheiser, *Clays Clay Miner.*, 1982, **30**, 97–102.
33 M. Jobbagy, F. Marino, B. Schobrod, G. Baronetti and M. Laborde, *Chem. Mater.*, 2006, **18**, 1945–1950.
34 D. G. Klissurski and E. L. Uzunova, *Chem. Mater.*, 1991, **3**, 1060–1063.
35 R. Xu and H. C. Zeng, *J. Phys. Chem. B*, 2003, **107**, 12643–12649.
36 Z. G. Zhao, F. X. Geng, J. B. Bai and H. M. Cheng, *J. Phys. Chem. C*, 2007, **111**, 3848–3852.
37 N. N. Nassar, *J. Hazard. Mater.*, 2010, **184**, 538–546.
38 S. L. Wan, X. Zhao, L. Lv, Q. Su, H. N. Gu, B. C. Pan, W. M. Zhang, Z. W. Lin and J. F. Luan, *Ind. Eng. Chem. Res.*, 2010, **49**, 7574–7579.
39 C. G. Rocha, D. A. M. Zaia, R. V. D. Alfaya and A. A. D. Alfaya, *J. Hazard. Mater.*, 2009, **166**, 383–388.
40 C. S. Kim, J. J. Rytuba and G. E. Brown, *J. Colloid Interface Sci.*, 2004, **271**, 1–15.

41 K. P. Lisha, S. M. Maliyekkal and T. Pradeep, *Chem. Eng. J.*, 2010, **160**, 432–439.
42 P. Arnfalk, S. A. Wasay and S. Tokunaga, *Water, Air, Soil Pollut.*, 1996, **87**, 131–148.
43 X. F. Wang and L. Andrews, *Inorg. Chem.*, 2005, **44**, 108–113.
44 X. M. Zhou, H. C. Yang, C. X. Wang, X. B. Mao, Y. S. Wang, Y. L. Yang and G. Liu, *J. Phys. Chem. C*, 2010, **114**, 17051–17061.
45 M. Y. Zhu and G. W. Diao, *J. Phys. Chem. C*, 2011, **115**, 18923–18934.
46 T. Fan, D. K. Pan and H. Zhang, *Ind. Eng. Chem. Res.*, 2011, **50**, 9009–9018.
47 J. Baltrusaitis, D. M. Cwiertny and V. H. Grassian, *Phys. Chem. Chem. Phys.*, 2007, **9**, 5542–5554.
48 A. P. Grosvenor, B. A. Kobe and N. S. McIntyre, *Surf. Sci.*, 2004, **572**, 217–227.
49 M. W. Roberts and P. R. Wood, *J. Electron Spectrosc. Relat. Phenom.*, 1977, **11**, 431–437.
50 S. J. Roosendaal, J. P. R. Bakker, A. M. Vredenberg and F. H. P. M. Habraken, *Surf. Sci.*, 2001, **494**, 197–205.
51 A. F. Carley, M. W. Roberts and A. K. Santra, *J. Phys. Chem. B*, 1997, **101**, 9978–9983.
52 X. Q. Li, J. S. Cao and W. X. Zhang, *Ind. Eng. Chem. Res.*, 2008, **47**, 2131–2139.
53 N. S. Mcintyre and D. G. Zetaruk, *Anal. Chem.*, 1977, **49**, 1521–1529.
54 S. H. Liu, R. M. Xing, F. Lu, R. K. Ran and J. J. Zhu, *J. Phys. Chem. C*, 2009, **113**, 21042–21047.